Perfect Extinction of Terahertz Waves in Monolayer Graphene over 2-nm-Wide Metallic Apertures

*Hyeong-Ryeol Park, Seon Namgung, Xiaoshu Chen, Nathan C. Lindquist, Vincenzo Giannini, Yan Francescato, Stefan A. Maier, and Sang-Hyun Oh**

High carrier mobility and tunability in graphene enable fundamental studies for plasmonics and various applications. Despite its versatility, however, single-layer graphene (SLG) suffers from poor coupling efficiency to electromagnetic waves, presenting a major challenge for photonic applications. Compared with visible or infrared radiation, terahertz (THz) waves exhibit higher absorption in SLG due to Drude-like intraband transitions, but the wavelength-to-SLG size mismatch becomes even more dramatic. Here, we experimentally demonstrate 99% extinction of THz wave transmission when SLG covers the openings of 2-nm-wide (≈λ/1 000 000) slits through a metal film. By resonantly coupling THz waves through annular nanogaps, the extremely localized fields lead to near-perfect extinction and strong absorption in SLG. Atomic-layer lithography is used to produce these nanometer-wide, millimeter-long gaps over an entire 4-in. wafer. Furthermore, by integrating these devices with an ionic liquid, enhanced intraband absorption in the SLG leads to 80% modulation of THz waves with an operational voltage as low as 1.5 V.

1. Introduction

Graphene[1] possesses unique optical properties[2–5] that enable exciting applications such as tunable metamaterials,[6,7] field-effect transistors,[8,9] optical modulators,[10–13] and photodetectors.[14,15] However, the extinction of transmitted light through single-layer graphene (SLG), which is caused by the sum of absorption and scattering, has been limited due to its inherent atomic-scale thickness. To enhance the optical absorption, SLG has been combined with subwavelength metallic apertures,[16] metamaterials,[7] multilayer graphene,[17] nanodisk arrays,[18] and photonic cavities.[19] Furthermore, various theoretical schemes have been proposed to attempt the ultimate feat in thin-film light-matter interactions—i.e., total absorption of light in monolayer graphene—using a photonic crystal slab,[20] and doped graphene nanodisks.[21] However, perfect optical extinction in monolayer graphene has not yet been demonstrated experimentally. One possible route to achieve perfect extinction in SLG is to squeeze electromagnetic waves through an extremely narrow aperture to maximize absorption of the graphene. Ideally, the gap size should be around a few nanometers to maximize the field enhancement in and around the graphene layer but not so small where tunneling across the gap would reduce the enhancement.[22] The nanogaps should also possess a mechanism to boost field intensity to compensate for the reduced transmission through the deeply subwavelength openings.

Dr. H.-R. Park, Dr. S. Namgung, X. Chen, Prof. S.-H. Oh
Department of Electrical and Computer Engineering
University of Minnesota
Minneapolis, MN 55455, USA
E-mail: sang@umn.edu
Prof. N. C. Lindquist
Physics Department
Bethel University
Saint Paul, MN 55112, USA
Dr. V. Giannini, Dr. Y. Francescato, Prof. S. A. Maier
Department of Physics
Imperial College London
London SW7 2AZ, UK

DOI: 10.1002/adom.201400546

2. Design and Fabrication

Recently, atomic-layer lithography[23–26] has been developed to overcome the technological challenge of fabricating nanometer-wide gaps along micrometer- to centimeter-scale loops. This method consists of a "plug-and-peel" metal patterning and atomic layer deposition (ALD) to define the lateral resolution of nanogaps. After a first pattern of gold (Au) is defined using standard photolithography, a conformal layer of alumina (Al_2O_3) is deposited on the vertical sidewalls and top surface of the patterned metal (**Figure 1**a). During this stage, the thickness of the alumina layer deposited on the sidewalls determines the lateral width of the vertically oriented gaps. After a second Au deposition (Figure 1b), the excess Au over the first metal patterns can be peeled off using an adhesive tape due to the weak adhesion between Au and Al_2O_3 (Figure 1c). The resulting nanogaps enabled the observation of huge field enhancements of over 25 000 with the amplitude transmittance of 50% when 4-mm wavelength electromagnetic waves were squeezed into the 1-nm wide (≈λ/4 000 000) metallic gaps, as reported in previous work.[24]

In the present work, we investigate how the highly confined and enhanced near-field generated in the vicinity of 2-nm-wide

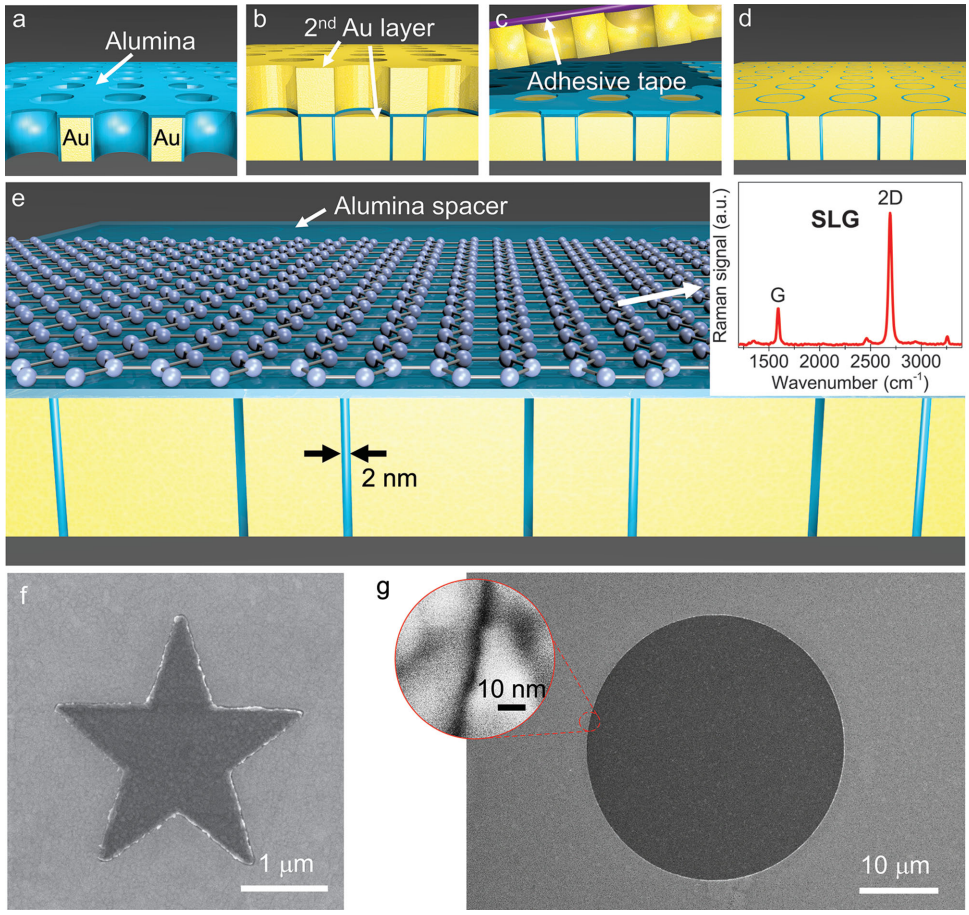

Figure 1. a) A circular hole array is fabricated into a thin gold film using standard lithography. The patterned metallic structure is conformally coated with a thin alumina (Al_2O_3) layer using atomic layer deposition (ALD). b) The holes are filled with gold by directional metal evaporation. c) Excess metal at the top surface is removed using an adhesive tape. The alumina layer is still partially covering the metal surface. d) To increase the surface sensitivity of the nanogap, the top alumina layer is etched by reactive ion etching (RIE). e) A CVD-grown SLG is transferred onto the annular gaps using standard transfer techniques. (Inset) Raman spectrum of SLG onto the patterned metallic film. f) Top-view scanning electron image (SEM) of a nanogap along a "star" shape. g) Top-view SEM of a 5-nm-wide annular gap. (Inset) The enlarged SEM image of the same 5 nm gap formed along the ring-shaped element.

gaps interact with atomically thin SLG in the terahertz (THz) regime. To place SLG directly over the nanogap, the remaining top alumina layer was removed via reactive ion etching (RIE) with an inductively coupled plasma (Plasmalab System100 ICP180, Oxford Ltd.) (Figure 1d). In the devices used for THz modulation, a uniform Al_2O_3 overlayer was grown on top of the metallic gaps using ALD to electrically tune the THz absorption in the SLG film. Lastly, CVD-grown SLG films were placed onto the samples using a standard transfer technique (Figure 1e) (for details of the transfer process, see Experimental Section). The graphene layer was characterized by confocal Raman spectroscopy (WITec alpha300 R confocal Raman microscope with UHTS300 spectrometer and DV401 CCD detector), as shown in Figure 1e (inset). The Raman spectra indicate a high quality SLG as attested by the locations of the G-peak (1593 cm^{-1}) and 2D-peak (2693 cm^{-1}), their intensity ratio (I_{2D}/I_G) of ≈3.5, and the full width at half maximum of the 2D-peak of about 40 cm^{-1}. Figure 1f demonstrates that the nanogaps can be formed along the contours of arbitrary shapes while Figure 1g shows a top-view scanning electron micrograph (SEM) of a 5-nm-wide annular gap with a diameter of 32 μm made through a 150-nm-thick Au film.

3. Results and Discussion

To experimentally probe the THz response of our graphene–nanogap hybrid structures, we performed THz time-domain spectroscopy (THz TDS)[24,27,28] on both a bare Pyrex glass substrate and the 2-nm-wide annular gaps with and without SLG (for details of THz-TDS, see Experimental Section). A linearly polarized THz wave is normally incident from the glass side underneath the annular gaps, which are polarization-independent structures with dipole resonances along the contour of each circular loop.[29] Surprisingly, placing SLG on top of these nanogaps without an alumina spacer almost completely shuts off the THz transmission (**Figure 2**a). The 32 μm diameter annular gaps were arranged in an array with a period of 50 μm through a 150-nm thick gold film (Figure 2b). Such a structure supports a bright dipole mode similar to a coaxial waveguide, as shown in Figure 2b (inset), which can be excited at the resonance frequency $f_{res} = c/(\ln_{eff})$, where c is speed of light, l is the perimeter of the annular gap, and n_{eff} is the effective index of the mode.[24,29]

In Figure 2c (top), the single cycle curve of the THz pulse through SLG on the bare Pyrex substrate remains intact,

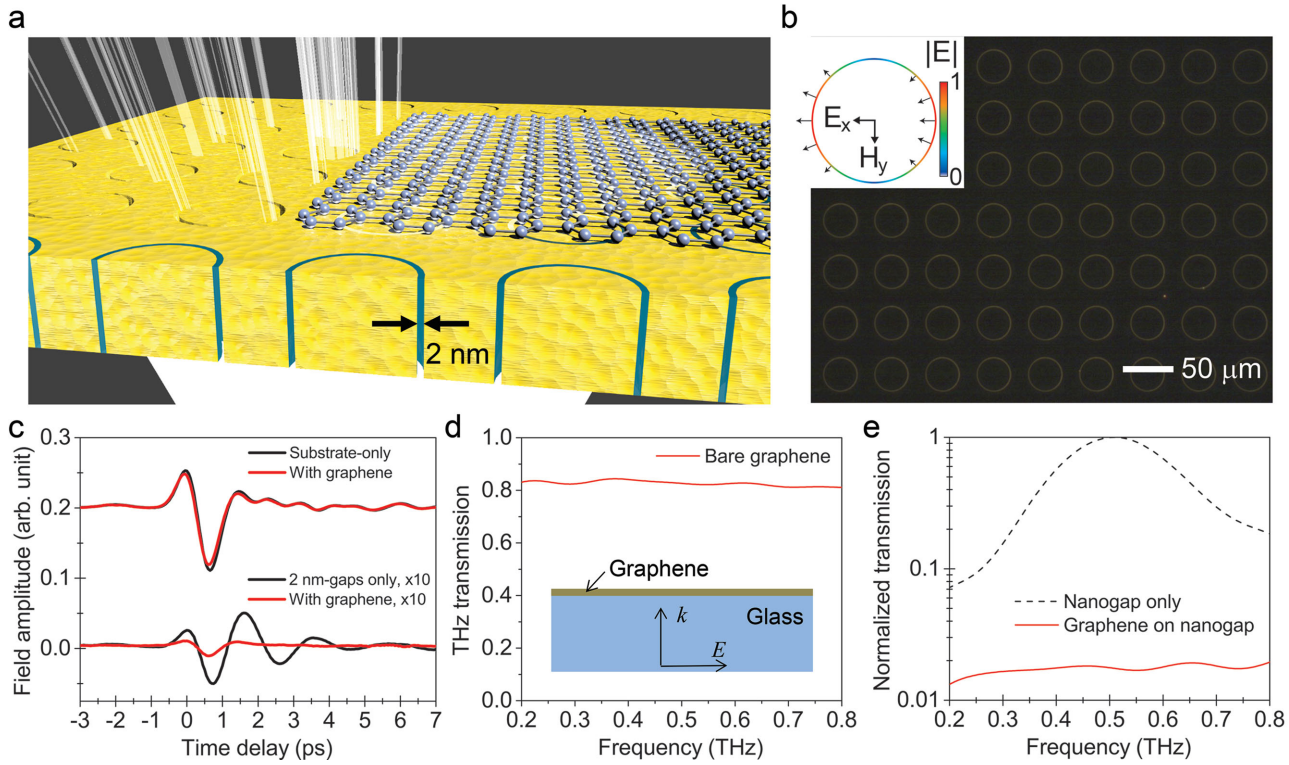

Figure 2. a) Schematic diagram of terahertz (THz) transmission coupled to SLG onto an annular gap array with a gap size of 2 nm. b) Top-view microscope image of annular gaps with a diameter of 32 μm and a period of 50 μm in a 150-nm thick Au film. (Inset) Illustration of the electric field distribution at a bright dipolar mode of the annular gap. The color scales show the amplitude of the field while the arrows show both the direction and amplitude of the field. c) Time-domain signals of transmitted electric field amplitudes for a bare glass substrate (top) and 2-nm wide annular gap array (bottom) without (black lines) and with (red lines) SLG. SLGs were directly contacted onto the metallic nanogap structure. The time traces are offset along the vertical axis for clarity. d) Fourier-transformed THz transmission spectrum through the SLG, normalized by the transmission through the bare substrate. e) Measured THz transmission spectra for the 2-nm wide annular gap array without (black dashed line) and with (red solid line) graphene. For easy comparison, we normalized the transmission amplitudes with the maximum value in the figure.

indicating little change between the peak-to-peak amplitudes of the substrate with and without SLG. The nanogap sample without SLG displays a quasi-periodic waveform, indicating strong THz resonance in the frequency domain (Figure 2c, bottom). Interestingly, for the nanogap sample with SLG, the periodic waveform is almost completely suppressed, resulting in a signal with a <20% peak-to-peak amplitude (Figure 2c, bottom). It is instructive to compare the Fourier transform transmission spectra to help us identify why the annular gaps give rise to so much extinction with SLG. While the graphene on the bare substrate shows a typical extinction of ≈20% over a broad THz frequency range[11] (Figure 2d), the 2-nm annular gaps with SLG allows 99% THz extinction leading to a reduction by another two orders of magnitude at the resonance frequency of 0.51 THz (Figure 2e). This huge extinction is mostly caused by absorption enhancement in SLG and large change of local refractive index around the nanogap enabled by SLG. Although it is difficult to quantify the contribution of each effect experimentally, numerical simulations show that SLG over the 2-nm gap can absorb 98% of total incident electromagnetic energy (See Supporting Information).

Also we experimentally show that this extinction is strongly dependent on the gap size—a critical parameter in determining the field enhancement around the gap.[24,28] Using THz time-domain spectroscopy, we measured THz transmissions through annular gaps, having different gap sizes of 2, 5, and 10 nm, without and with SLG, as shown in **Figure 3**a–c. Two interesting features in this result are that: i) the THz extinction decreases for the increasing gap size (Figure 3d) and, ii) for gaps wider than 2 nm, which do not show perfect extinction of the THz resonance peak, we observe that the transmission peak with SLG shifts toward lower frequencies, compared with the peak without SLG. This is experimental evidence showing that the absorption enhancement, which is proportional to the field intensity near the gap, increases as the gap size decreases.[30] Furthermore, the resonant transmission through the annular gap is strongly influenced by the refractive indices of the upper and bottom media of the gap, as well as the index inside the gap. While the index value of the 500-μm-thick glass substrate is constant, the 2-nm gap can further increase the effective index value of the upper medium—graphene and air—because of its stronger field confinement than those of the wider gaps (5 and 10 nm).[31,32] In addition to the strong absorption in the SLG, transmission is also affected by an impedance mismatch between the graphene layer and the nanogap as well as absorption in the metal. However, our simulations (Figure S1, Supporting Information) showed that the majority of the energy lost is due to the SLG only.

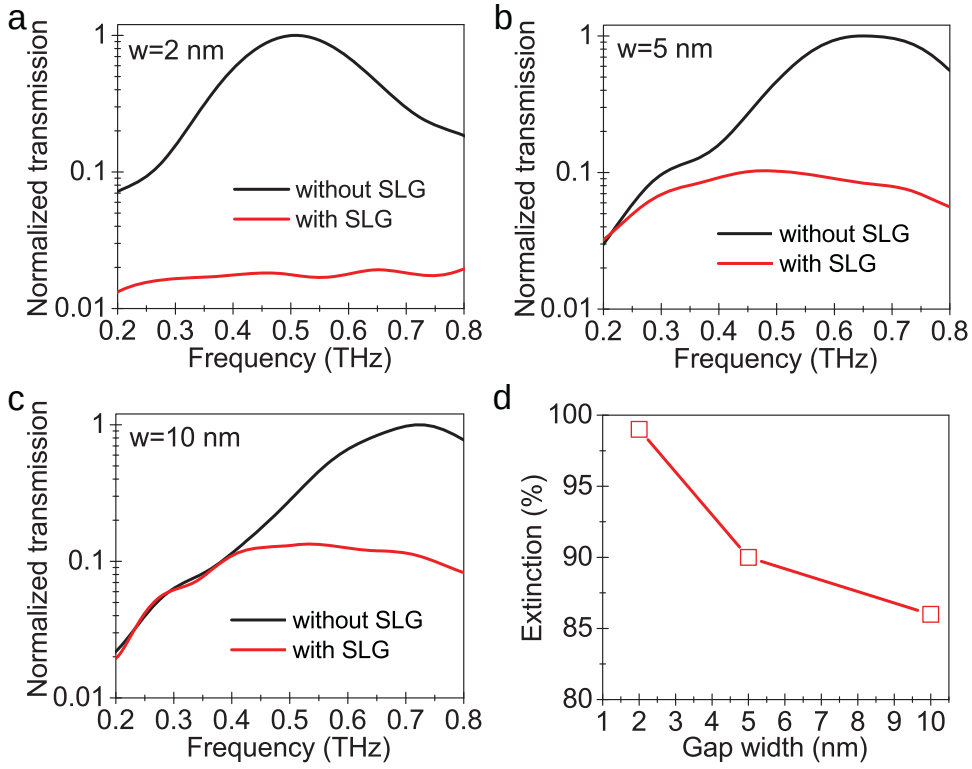

Figure 3. Measured THz transmission (log-scale) through 32 μm diameter annular gaps, having the gap sizes (w) of a) 2, b) 5, and c) 10 nm, without (black line) and with (red line) SLG. For easy comparison, we normalized the transmission amplitudes with the maximum value in each figure. d) THz extinction of the graphene–nanogap hybrid structure at the resonance as a function of the gap size.

Because of such strong light–matter interactions in our devices, the confinement of THz waves inside 2-nm-wide slits also enables high-contrast modulation of THz transmission using SLG. For such modulation experiments, we had to insert a spacer between SLG and the metallic nanogaps as described above. This allowed an electrically controllable hybrid material platform, consisting of the 2-nm-wide annular gaps, a SLG film, and an ionic liquid layer[18] on top of the SLG film (**Figure 4**a). 1-Butyl-3-methylimidazolium hexafluorophosphate ([BMI][PF6]) was used as the ionic liquid layer to yield a high capacitance (3.9 μF cm^{-2})[33] and a low absorption in the THz frequency region. The ionic liquid was injected in a microfluidic channel made of a cover glass and double-sided Scotch tape as a spacer. A platinum (Pt) wire as a top gate electrode was connected to the ionic liquid layer, and two gold electrodes were put on both sides of the ≈12 mm × 6 mm SLG film (Figure 4a). A gate voltage (V_g) was applied between the top Pt electrode and one Au electrode on graphene in the range −1.5 to 1.5 V, and a bias voltage (V_b) was applied between both of the Au electrodes on the SLG with 0.1 V at the same time to monitor the DC current/resistance of the SLG. A 2-nm-thick alumina spacer was added by ALD between the top surface of the nanogap structure and the SLG layer in order to enhance the THz modulation depth controlled by a top gate voltage (Figure 4a (inset)). Unlike the SLG in direct contact with the nanogaps in Figure 2, the peak transmission of the hybrid switching device with the additional alumina spacer at $V_g = 0$ V is about 20% that of the bare nanogap sample, as shown in Figure 4b.

To change the carrier density in SLG, we applied the top gate voltage and observed the resulting THz transmissions and DC currents simultaneously. As the gate voltage increases from −1.5 V to 1.5 V, maximum THz transmission (red triangle line) at a fixed frequency of 0.5 THz is observed at $V_g = 0.3$ V, indicating that the Fermi energy at this gate voltage is closest to the Dirac point, as shown in Figure 4c. The DC current (orange circle line) also shows the lowest value at the same voltage, confirming the Dirac point of the SLG. Furthermore, the hybrid graphene–nanogap device shows a hysteretic behavior in the THz transmission for a cycle of the gate voltage due to charge carrier retention, potentially allowing photonic memory applications.[7,34] As the gate voltage decreases from −0.1 V to −1.5 V, the largest THz modulation depth of ≈80% is observed at the specific frequency of 0.5 THz. This is to the best of our knowledge a record for SLG applications.

The Fermi energy level of the SLG can be estimated using a simple capacitor model[35] as $\left|E_F(V_g)\right| = \hbar v_F \sqrt{\pi n}$, where $E_F(V_g)$ is the Fermi energy at the gate voltage V_g, $\hbar$ is the reduced Plank constant, $v_F = 10^6$ m s^{-1} is the Fermi velocity of Dirac fermions, and n is the carrier density calculated by $n = C\left|V_g - V_{CNP}\right|/e$, where C is the capacitance of the ionic liquid layer, e is the electron charge, and V_{CNP} is taken as 0.3 V, the closest value to the Dirac point. Figure 4d shows the gate voltage dependence of the Fermi energy obtained through the capacitor model.[18]

To further elucidate the physical mechanisms responsible for the observed THz extinction in SLG over the nanogap, we performed 2D COMSOL modeling with infinitely long nano-slits

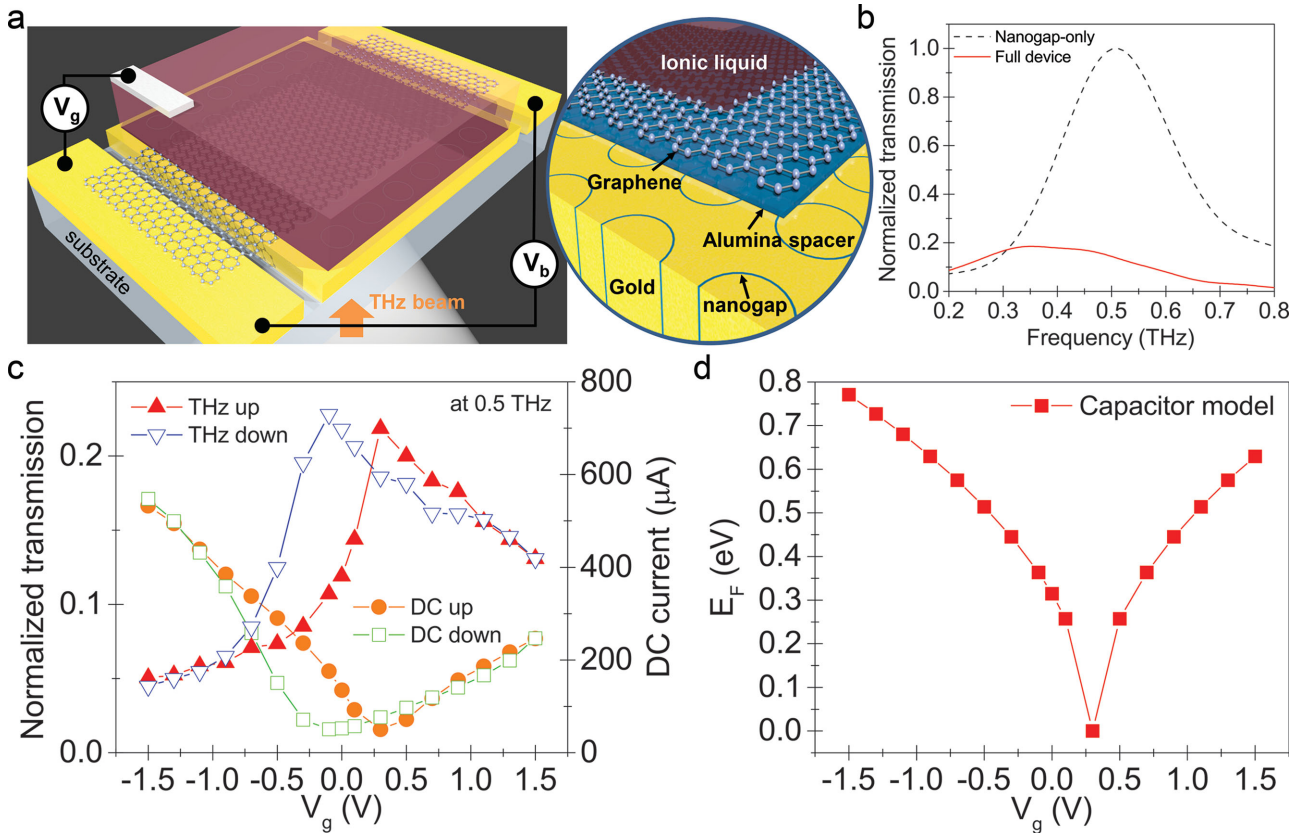

Figure 4. a) Illustration of our graphene–nanogap hybrid device with a high capacitance ionic liquid. The ionic liquid was injected into a microfluidic channel on the graphene. A platinum wire as a top gate is connected to the ionic liquid. A gate voltage, V_g, was applied between one Au electrode on graphene and the platinum wire. A bias voltage, V_b, was applied between both of the Au electrodes on graphene at the same time to monitor the dc current of graphene. The THz pulses are normally incident on the sample. (Inset) A 2-nm thick alumina spacer is used between SLG and the 2-nm wide annular gaps, in order to permit the electrical tunability of the THz transmission through our hybrid device. b) THz transmission spectra of the 2-nm wide annular gap array only (black dashed line) and the hybrid device with the same nanogap structure (red solid line), normalized by the peak value of the transmission through the nanogap only. c) Normalized THz transmission of our nanogap device (red and blue lines) and dc current (orange and green lines) as a function of gate voltage. "up" ("down") in the legend means measured values as the gate voltage increases (decreases) from –1.5 (+1.5) to +1.5 (–1.5) V. d) The absolute value of the Fermi energy E_F versus gate voltage V_g estimated using a simple capacitor model.

(for details of the numerical simulations, see Experimental Section). To reduce computational complexity, the SLG is treated as an effective medium with a thickness of 2 nm.[36,37] The permittivity of the 2-nm-thick medium for SLG is given by $\varepsilon = 1 + (i\sigma)/(\varepsilon_0 \omega t)$, where σ is the effective conductivity of the graphene, ε_0 is the vacuum permittivity, ω is the angular frequency of the light, and t (=2 nm) is the effective thickness of the SLG film.[36,37]

In **Figure 5**a,b, the surface conductivity and effective refractive index of the graphene over the frequency range 0.1–1.0 THz were estimated using the local random phase approximation of the Kubo formula[38] considering both the intraband and interband contributions at the temperature T = 300 K, the Fermi energy E_F = 0.3 eV, and the scattering rate Γ = 0.1 eV.[35] In Figure 5c,d, we compare electric field enhancement factors of 5-nm-wide slits both without and with the SLG layer with the effective refractive index calculated in Figure 5b. While the field amplitude ($|E|$) enhancement factor without graphene is about 700, the enhancement factor for the gap with the graphene dramatically shrinks to below 50, leading to 99% extinction of THz wave intensity ($|E|^2$). This result has a good quantitative agreement with the experimental results shown in Figure 3b,d. Furthermore, by adding the 2-nm-thick alumina spacer between the graphene and the nanogap in the simulation, the averaged intensity ($|E|^2$) enhancement at the exit of the gap can be modulated by 52% as the Fermi energy of graphene is changed from 0.01 to 0.8 eV (Figure 5e,f). While this value is lower than the experimental results shown in Figure 4, this can be attributed to the lower (non-resonant) field enhancements of the infinitely long slits used in the simulations. However, we emphasize the remarkably good agreement between these simulations and experiments, demonstrating the strong interaction between THz waves and SLG with the nanogap.

4. Conclusion

Experimental demonstration of near-perfect THz extinction in SLG with our 2 nm gaps opens up new and exciting possibilities to construct graphene–nanogap hybrid device for various applications. As an example, we showed a wafer-scale graphene-over-nanogap architecture that displayed high-contrast THz

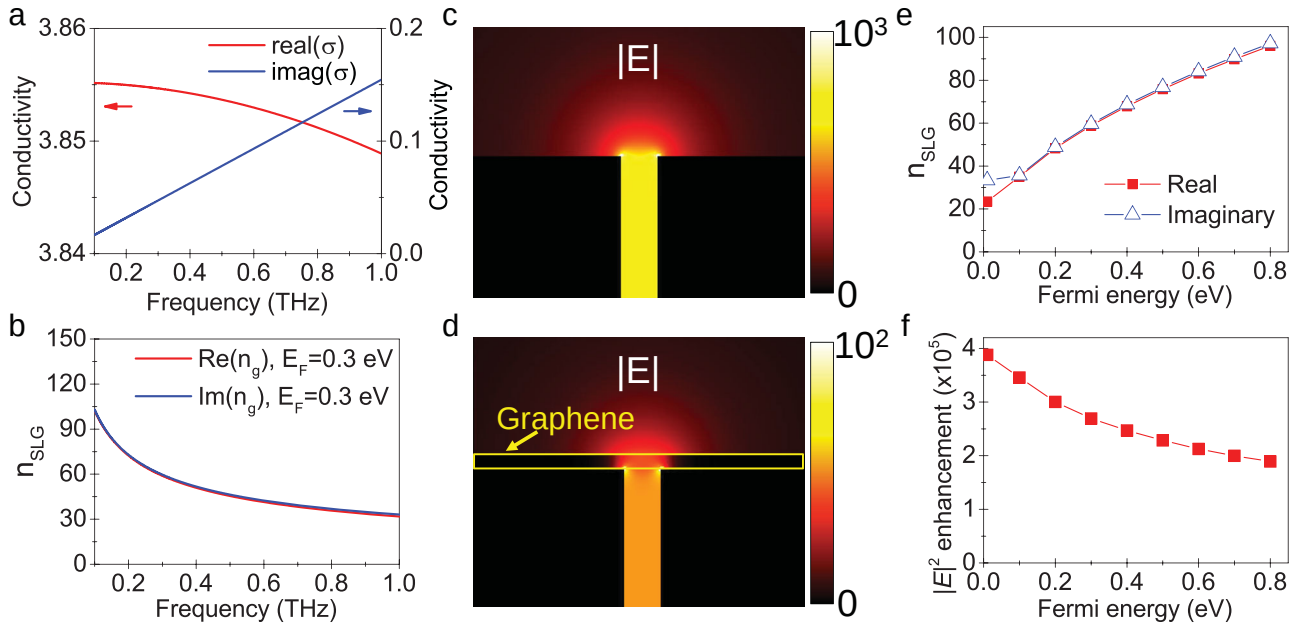

Figure 5. a) Real (red, left) and imaginary (blue, right) parts of the conductivity for graphene at $T = 300$ K with $E_F = 0.3$ eV and $\Gamma = 0.1$ eV. The unit of conductivity is $\pi G_0/4 = 6.08 \times 10^{-5}$ S. b) Real (red lines) and imaginary (blue lines) parts of the effective refractive index for SLG with an effective thickness of 2.0 nm at $E_F = 0.3$ eV. c,d) Calculated electric field enhancements (FE) around a 5 nm-wide slit in a 150 nm-thick gold film without (FE = 700, c)) and with (FE = 50, d)) the SLG (modeled in b) at $E_F = 0.3$ eV) at the wavelength of 1 mm ($f = 0.3$ THz). Fields were determined using a 2D COMSOL simulation. e) At the 0.3 THz, effective refractive index of the graphene versus its Fermi energy. f) Averaged intensity ($|E|^2$) enhancement at the exit of the gap as a function of the Fermi energy of the graphene, including a 2-nm thick alumina spacer onto the nanogap.

wave modulation as large as ≈80% with an operational voltage of only 1.5 V. Furthermore, because the tightly confined THz wave near the nanogap can detect the changes of local refractive index enabled by the monolayer graphene, our nanogap paves a way toward THz sensing of atomically thin films, such as graphene or MoS_2, self-assembled monolayer, and biomolecules. Together, our results provide powerful new techniques for developing optical modulators,[39–42] or investigating novel nonlinear[39,43] and optical rectification[44] phenomena.

5. Experimental Section

Graphene Transfer over Nanogap Array: We purchased the CVD-grown SLG film on copper foil from a commercial vendor (Graphene Laboratories Inc.). For the transfer process, we spin-coated a poly(methyl methacrylate) (PMMA) layer onto graphene, and etched the copper foil in 1 M ammonium persulfate. After rinsing the etchant residue from the PMMA–graphene film, the PMMA–graphene film was scooped by the substrate. The samples were dried overnight, the PMMA was removed with acetone, and the whole sample was then cleaned with isopropyl alcohol (IPA).

Terahertz Time-Domain Spectroscopy: We measured the transmission spectra of the annular gap array in the frequency range from 0.1 THz to 1.5 THz using THz time-domain spectroscopy. In our setup, a femtosecond Ti:Sapphire laser (Mai-Tai XF, Newport Corporation) illuminated a GaAs-based photoconductive antenna (Tera-SED, Gigaoptics, GmbH) with a pulse train of wavelength 780 nm, 80 MHz repetition rate, and 90-fs pulse width. The *p*-polarized millimeter-wavelength pulses were normally incident on the annular gap structure. The THz waves transmitted through the annular gaps were collected using a Tsurupica lens (NA = 0.45) and detected via electro-optic sampling using a (110)-oriented ZnTe crystal.

2D Finite-Element Method Modeling Using COMSOL: We numerically simulated infinitely long slits with gap sizes of 2 and 5 nm in a 150 nm-thick gold film using COMSOL. The Drude model was used to fit the optical parameters of the gold film (plasma frequency of 1.37×10^4 THz, damping parameter of 40.7 THz) in THz frequencies.[45] The thickness dependent refractive indices of the 5 nm and 2 nm thick alumina films were 2.12 and 1.73, respectively.[24] The refractive index of the glass substrate was 1.95. Due to the extreme length-scale differences between the millimeter waves and nanometer gaps, care was taken to mesh the simulation area properly. The largest element size in free space was 20 μm whereas the smallest element size was 0.1 nm in the gap. The simulation area covered 9 mm high × 6 mm wide. Perfectly matched layers (PML) were used to minimize boundary reflections with plane-wave THz illumination from the glass substrate side. Field enhancements within the gap were calculated by comparing the average amplitude within the gap to a reference amplitude, which was the transmitted electric field amplitude through the interface between air and glass without the nanogap or gold film.

Supporting Information

Supporting Information is available from the Wiley Online Library or from the author.

Acknowledgements

This work was supported by the U.S. Department of Defense (DARPA Young Faculty Award N66001-11-1-4152; X.S.C., H.R.P., S.-H.O.), the Engineering and Physical Sciences Research Council and the Leverhulme Trust (V.G., Y.F., S.A.M.). Device fabrication was performed at the University of Minnesota, Nanofabrication Center, which receives support from the National Science Foundation (NSF) through the

National Nanotechnology Infrastructure Network program, and the Characterization Facility, which has received capital equipment funding from NSF through the Materials Research Science and Engineering Center. S.-H.O. also acknowledges support from the Office of Naval Research Young Investigator Award.

Received: November 13, 2014
Revised: December 3, 2014
Published online: January 7, 2015

[1] A. H. Castro Neto, F. Guinea, N. M. R. Peres, K. S. Novoselov, A. K. Geim, *Rev. Mod. Phys.* **2009**, *81*, 109.
[2] A. N. Grigorenko, M. Polini, K. S. Novoselov, *Nat. Photonics* **2012**, *6*, 749.
[3] J. N. Chen, M. Badioli, P. Alonso-Gonzalez, S. Thongrattanasiri, F. Huth, J. Osmond, M. Spasenovic, A. Centeno, A. Pesquera, P. Godignon, A. Z. Elorza, N. Camara, F. J. G. de Abajo, R. Hillenbrand, F. H. L. Koppens, *Nature* **2012**, *487*, 77.
[4] Z. Fei, A. S. Rodin, G. O. Andreev, W. Bao, A. S. McLeod, M. Wagner, L. M. Zhang, Z. Zhao, M. Thiemens, G. Dominguez, M. M. Fogler, A. H. C. Neto, C. N. Lau, F. Keilmann, D. N. Basov, *Nature* **2012**, *487*, 82.
[5] T. Low, P. Avouris, *ACS Nano* **2014**, *8*, 1086.
[6] L. Ju, B. S. Geng, J. Horng, C. Girit, M. Martin, Z. Hao, H. A. Bechtel, X. G. Liang, A. Zettl, Y. R. Shen, F. Wang, *Nat. Nanotechnol.* **2011**, *6*, 630.
[7] S. H. Lee, M. Choi, T. T. Kim, S. Lee, M. Liu, X. Yin, H. K. Choi, S. S. Lee, C. G. Choi, S. Y. Choi, X. Zhang, B. Min, *Nat. Mater.* **2012**, *11*, 936.
[8] K. S. Novoselov, A. K. Geim, S. V. Morozov, D. Jiang, Y. Zhang, S. V. Dubonos, I. V. Grigorieva, A. A. Firsov, *Science* **2004**, *306*, 666.
[9] I. Maeng, S. Lim, S. J. Chae, Y. H. Lee, H. Choi, J. H. Son, *Nano Lett.* **2012**, *12*, 551.
[10] M. Liu, X. B. Yin, X. Zhang, *Nano Lett.* **2012**, *12*, 1482.
[11] B. Sensale-Rodriguez, R. S. Yan, M. M. Kelly, T. Fang, K. Tahy, W. S. Hwang, D. Jena, L. Liu, H. G. Xing, *Nat. Commun.* **2012**, *3*, 780.
[12] N. K. Emani, T. F. Chung, A. V. Kildishev, V. M. Shalaev, Y. P. Chen, A. Boltasseva, *Nano Lett.* **2014**, *14*, 78.
[13] L. Shao, X. M. Wang, H. T. Xu, J. F. Wang, J. B. Xu, L. M. Peng, H. Q. Lin, *Adv. Opt. Mater.* **2014**, *2*, 162.
[14] F. N. Xia, T. Mueller, Y. M. Lin, A. Valdes-Garcia, P. Avouris, *Nat. Nanotechnol.* **2009**, *4*, 839.
[15] X. T. Gan, R. J. Shiue, Y. D. Gao, I. Meric, T. F. Heinz, K. Shepard, J. Hone, S. Assefa, D. Englund, *Nat. Photonics* **2013**, *7*, 883.
[16] W. Gao, J. Shu, K. Reichel, D. V. Nickel, X. He, G. Shi, R. Vajtai, P. M. Ajayan, J. Kono, D. M. Mittleman, Q. Xu, *Nano Lett.* **2014**, *14*, 1242.
[17] G. Pirruccio, L. M. Moreno, G. Lozano, J. G. Rivas, *ACS Nano* **2013**, *7*, 4810.
[18] Z. Y. Fang, Y. M. Wang, A. E. Schather, Z. Liu, P. M. Ajayan, F. J. G. de Abajo, P. Nordlander, X. Zhu, N. J. Halas, *Nano Lett.* **2014**, *14*, 299.
[19] B. Sensale-Rodriguez, R. S. Yan, S. Rafique, M. D. Zhu, W. Li, X. L. Liang, D. Gundlach, V. Protasenko, M. M. Kelly, D. Jena, L. Liu, H. G. Xing, *Nano Lett.* **2012**, *12*, 4518.
[20] J. R. Piper, S. Fan, *ACS Photonics* **2014**, *1*, 347.
[21] S. Thongrattanasiri, F. H. Koppens, F. J. Garcia de Abajo, *Phys. Rev. Lett.* **2012**, *108*, 047401.
[22] R. Esteban, A. G. Borisov, P. Nordlander, J. Aizpurua, *Nat. Commun.* **2012**, *3*, 825.
[23] H. Im, K. C. Bantz, N. C. Lindquist, C. L. Haynes, S.-H. Oh, *Nano Lett.* **2010**, *10*, 2231.
[24] X. Chen, H. R. Park, M. Pelton, X. Piao, N. C. Lindquist, H. Im, Y. J. Kim, J. S. Ahn, K. J. Ahn, N. Park, D. S. Kim, S.-H. Oh, *Nat. Commun.* **2013**, *4*, 2361.
[25] X. Chen, H.-R. Park, N. C. Lindquist, J. Shaver, M. Pelton, S.-H. Oh, *Sci. Rep.* **2014**, *4*, 6722.
[26] X. Chen, C. Ciraci, D. R. Smith, S.-H. Oh, *Nano Lett.* **2014**, DOI: 10.1021/nl503126s.
[27] D. Grischkowsky, S. Keiding, M. Vanexter, C. Fattinger, *J. Opt. Soc. Am. B* **1990**, *7*, 2006.
[28] M. A. Seo, H. R. Park, S. M. Koo, D. J. Park, J. H. Kang, O. K. Suwal, S. S. Choi, P. C. M. Planken, G. S. Park, N. K. Park, Q. H. Park, D. S. Kim, *Nat. Photonics* **2009**, *3*, 152.
[29] J. Shu, C. Y. Qiu, V. Astley, D. Nickel, D. M. Mittleman, Q. F. Xu, *Opt. Express* **2011**, *19*, 26666.
[30] H. R. Park, K. J. Ahn, S. Han, Y. M. Bahk, N. Park, D. S. Kim, *Nano Lett.* **2013**, *13*, 1782.
[31] F. J. Garcia-Vidal, E. Moreno, J. A. Porto, L. Martin-Moreno, *Phys. Rev. Lett.* **2005**, *95*, 103901.
[32] M. Seo, J. Kyoung, H. Park, S. Koo, H. S. Kim, H. Bernien, B. J. Kim, J. H. Choe, Y. H. Ahn, H. T. Kim, N. Park, Q. H. Park, K. Ahn, D. S. Kim, *Nano Lett.* **2010**, *10*, 2064.
[33] C. Merlet, M. Salanne, B. Rotenberg, P. A. Madden, *Electrochim. Acta* **2013**, *101*, 262.
[34] T. Driscoll, H. T. Kim, B. G. Chae, B. J. Kim, Y. W. Lee, N. M. Jokerst, S. Palit, D. R. Smith, M. Di Ventra, D. N. Basov, *Science* **2009**, *325*, 1518.
[35] L. Ren, Q. Zhang, J. Yao, Z. Z. Sun, R. Kaneko, Z. Yan, S. Nanot, Z. Jin, I. Kawayama, M. Tonouchi, J. M. Tour, J. Kono, *Nano Lett.* **2012**, *12*, 3711.
[36] A. Vakil, N. Engheta, *Science* **2011**, *332*, 1291.
[37] Y. Francescato, V. Giannini, S. A. Maier, *New J. Phys.* **2013**, *15*, 063020.
[38] A. Y. Nikitin, F. Guinea, F. J. Garcia-Vidal, L. Martin-Moreno, *Phys. Rev. B* **2011**, *84*, 195446.
[39] M. K. Liu, H. Y. Hwang, H. Tao, A. C. Strikwerda, K. B. Fan, G. R. Keiser, A. J. Sternbach, K. G. West, S. Kittiwatanakul, J. W. Lu, S. A. Wolf, F. G. Omenetto, X. Zhang, K. A. Nelson, R. D. Averitt, *Nature* **2012**, *487*, 345.
[40] L. Y. Deng, J. H. Teng, H. W. Liu, Q. Y. Wu, J. Tang, X. H. Zhang, S. A. Maier, K. P. Lim, C. Y. Ngo, S. F. Yoon, S. J. Chua, *Adv. Opt. Mater.* **2013**, *1*, 128.
[41] S. Savo, D. Shrekenhamer, W. J. Padilla, *Adv. Opt. Mater.* **2014**, *2*, 275.
[42] H. R. Seren, G. R. Keiser, L. Cao, J. Zhang, A. C. Strikwerda, K. Fan, G. D. Metcalfe, M. Wraback, X. Zhang, R. D. Averitt, *Adv. Opt. Mater.* **2014**, *2*, 1221.
[43] H. Y. Hwang, N. C. Brandt, H. Farhat, A. L. Hsu, J. Kong, K. A. Nelson, *J. Phys. Chem. B* **2013**, *117*, 15819.
[44] D. R. Ward, F. Huser, F. Pauly, J. C. Cuevas, D. Natelson, *Nat. Nanotechnol.* **2010**, *5*, 732.
[45] M. A. Ordal, L. L. Long, R. J. Bell, S. E. Bell, R. R. Bell, R. W. Alexander, C. A. Ward, *Appl. Opt.* **1983**, *22*, 1099.